



Two Film Approach to Continuum Scale Mixing and Dispersion with Equilibrium Bimolecular Reaction

Simon A. Mathias¹ · Diogo Bolster² · Sergii Veremieiev¹

Received: 16 January 2024 / Accepted: 3 May 2024 / Published online: 27 May 2024
© The Author(s) 2024

Abstract

Reliable reactive transport models require careful separation of mixing and dispersion processes. Here we treat displacing and displaced fluids as two separate fluid phases and invoke Whitman's classical two-film theory to model mass transfer between the two phases. We use experimental data from Gramling's bimolecular reaction experiment to assess model performance. Gramling's original model involved just three coupled PDEs. In this context, our new formulation leads to a set of seven coupled PDEs but only requires the specification of two extra parameters, associated with the mass transfer coefficient and its dependence on time. The two film mass transfer model provides a simple and theoretically based method for separating mixing from dispersion in Eulerian continuum-scale methods. The advantage of this approach over existing methods is that it enables the simulation of equilibrium chemical reactions without having to invoke unrealistically small reaction rate coefficients. The comparison with Gramling's experimental data confirms that our proposed method is suitable for simulating realistic and complicated bimolecular reaction behaviour. However, further work is needed to explore alternative methods for avoiding the need of a time-dependent mass transfer rate coefficient.

Keywords Mixing · Dispersion · Two film theory · Bimolecular reaction

1 Introduction

The advection dispersion equation (ADE) is widely used to simulate continuum scale solute transport in porous media. In this context, the dispersion term commonly takes the form of a Fickian diffusion operator. The associated dispersion coefficient is typically taken to be

✉ Simon A. Mathias
s.a.mathias@durham.ac.uk

Diogo Bolster
dbolster@nd.edu

Sergii Veremieiev
s.veremieiev@durham.ac.uk

¹ Department of Engineering, Durham University, Durham, UK

² Department of Civil and Environmental Engineering, University of Notre Dame, Notre Dame, IN, USA

a linear function of pore-fluid velocity, with the coefficient of proportionality referred to as the dispersivity. The dispersivity is a characteristic property thought to describe the extent to which solutes are spread due to sub-continuum scale heterogeneity in flow velocities.

Notwithstanding the many shortcomings associated with such Fickian dispersion models for describing non-reactive transport, a particular problem arises in the context of reactive transport. The issue is that dissolved chemicals only react with each other when direct contact is made, which in turn is achieved by the mixing of fluids. Within the ADE, mixing takes place due to molecular diffusion. Unfortunately, the ADE is unable to distinguish between dispersion and diffusion; spreading and mixing are treated as the same process. Given that dispersion coefficients are generally orders of magnitude larger than molecular diffusion coefficients, the ADE therefore significantly overestimates extent of mixing, leading to a corresponding overestimate of reaction rate.

This latter point is demonstrated by the combined experimental and modelling study of Gramling et al. (2002). They performed a series of sand column experiments involving the displacement of water containing $\text{Na}_2\text{EDTA}^{2-}$ by water containing CuSO_4 . The two chemicals react on contact to form CuEDTA^{2-} . The reaction kinetics are sufficiently fast (compared to the transport processes) that it is considered reasonable to treat them as equilibrium processes. Their ADE model overestimated the amount of CuEDTA^{2-} produced by around 20%.

Many alternative models have since been promoted to more appropriately distinguish between mixing and spreading. The experimental observations from Gramling et al. (2002) are frequently used to demonstrate the efficacy of new approaches. Gramling et al. (2002) reports time-series results for CuEDTA^{2-} production for three different column flow rates (2.67 ml min^{-1} , 16 ml min^{-1} and 150 ml min^{-1}). Additionally they provide spatial distribution of CuEDTA^{2-} concentrations after 619, 916, 1114 and 1510 s for their 2.67 ml min^{-1} column experiment, after 157 s for their 16 ml min^{-1} column experiment and after 20.23 s for their 150 ml min^{-1} column experiment.

Modelling approaches applied include both Lagrangian particle tracking (LPT) methods (Edery et al. 2009, 2010; Ding et al. 2013; Alhashmi et al. 2015; Sole-Mari et al. 2020) and Eulerian continuum-scale (ECS) methods (Sanchez-Vila et al. 2010; Zhang et al. 2013; Barnard 2017; Ginn 2018; Gurung and Ginn 2020; Sole-Mari et al. 2022). LPT methods have the special advantage of providing a general framework for describing stochastic processes characterised by a wide range of different statistical distributions. Nevertheless, ECS methods persist in being the preferred option when studying contaminant transport for practical and applied purposes (e.g. Diersch 2013; Simunek et al. 2016; Jung et al. 2017; Voss et al. 2010). ECS approaches that seek to distinguish between spreading and mixing are therefore certainly worth pursuing further.

Sanchez-Vila et al. (2010) simulated Gramling's 2.67 ml min^{-1} column experiment using the ADE with a first-order kinetic term for the reaction process, which considers the product of the $\text{Na}_2\text{EDTA}^{2-}$ and CuSO_4 concentrations. Their model closely matched the experimental data in terms of both the four CuEDTA^{2-} concentration profiles and the time-series data for CuEDTA^{2-} production. They treated the reaction rate coefficient (RRC) as a power law of time, requiring the calibration of two additional parameters (as compared to the equilibrium model originally used by Gramling et al. 2002).

Gramling et al. (2002) state that the reaction rate coefficient (RRC) for this process is $2.3 \times 10^9 \text{ M}^{-1}\text{s}^{-1}$. The value of RRC adopted by Sanchez-Vila et al. (2010) declined with time and after just 1 s would have reached $240 \text{ M}^{-1}\text{s}^{-1}$. Sanchez-Vila et al. (2010) argue that this slower RRC incorporates the effect of incomplete mixing at the continuum scale

by lumping together the local-scale reaction rate with the rate of mass transfer between two regions, one containing the displaced fluid and the other containing the displacing fluid. They introduced a time-dependency for the RRC on the basis of experimental evidence, previously presented by Haggerty et al. (2004), demonstrating how two-region mass transfer coefficients, for transport in porous media, tend to decline with time. However, there are no established upscaling theories to provide a physical basis for combining multi-region mass transfer processes into a larger RRC in this way.

Zhang et al. (2013) revisited the study of Sanchez-Vila et al. (2010) and incorporated an additional reverse reaction rate coefficient (also treated as a power law of time), enabling the kinetic reaction term to also include the CuEDTA^{2-} solute concentration. Whilst they were able to achieve modest reductions in the error between the observed and modelled data, their RRC remained several orders of magnitude less than the $2.3 \times 10^9 \text{ M}^{-1}\text{s}^{-1}$ estimated by Gramling et al. (2002).

Barnard (2017) sought to separate out the mass transfer process and reaction rate by explicitly distinguishing between mixed and unmixed solutes. They introduced two RRCs. One of the RRC described the rate at which unmixed solute is transformed to being mixed solute, the other was used to describe the CuEDTA^{2-} production. Values of both RRCs were obtained by calibrating their model to the CuEDTA^{2-} concentration profile data from Gramling's 2.67 ml min^{-1} column experiment. Unfortunately, Barnard (2017) found that they needed to adopt a CuEDTA^{2-} RRC, which was 10 orders of magnitude less than originally determined by Gramling et al. (2002).

Ginn (2018) and Gurung and Ginn (2020) modified the linear kinetic mixing model of Barnard (2017) by forcing the associated RRC to decline with the square-root of time (implicitly linked to the aforementioned findings of Haggerty et al. 2004). Importantly, Ginn (2018) was able to match the CuEDTA^{2-} concentration profile data from Gramling's 2.67 ml min^{-1} column experiment whilst maintaining the CuEDTA^{2-} reaction as an equilibrium process. However, there is no physical basis for treating mixing as a kinetic reaction process in this context. Here we propose an alternative approach based on the classical two-film theory of Whitman (Lewis and Whitman 1924), commonly associated with partially miscible displacement problems.

Mass transfer of chemicals from one fluid phase to another can be described by a combination of molecular diffusion and Henry's law. Whitman's two-film theory hypothesises that diffusion occurs only within two thin films either side of a phase interface. Outside of the films, solute concentrations are assumed to be locally uniform within each phase. It can then be shown that mass transfer of a solute from one phase to another is a linear function of the concentration difference between the two phases.

Our hypothesis is that Whitman's two-film theory should also apply to fully miscible displacement problems. In this case, Henry's law is no longer needed and the two fluid phases are represented by the displaced and displacing fluids. In reality, both the displaced and displacing fluids belong to the same fluid phase. However, from a modelling perspective, they exhibit distinct characteristics akin to different phases due to their relative motion and compositional differences. By treating the two fluids as distinctly separate entities, we can utilise Whitman's two-film theory to explicitly distinguish between mixing and spreading. Mixing is described by mass transfer between the two fluids, while spreading is described by dispersion within the two fluids.

Previous researchers (Barnard 2017; Ginn 2018; Gurung and Ginn 2020) distinguished between unmixed and mixed chemical components. We are alternatively distinguishing between displacing and displaced fluids, allowing us to represent a process that is much closer to reality. Previous researchers assumed that rate of mass transfer from an "unmixed state" to

a “mixed state” is linearly proportional to the solute concentration of the “unmixed state”. We are instead assuming that rate of mass transfer from a displacing fluid to a displaced fluid is linearly proportional to the solute concentration difference between displacing and displaced fluids. Whereas the mixing rate coefficients adopted by Barnard (2017), Ginn (2018) and Gurung and Ginn (2020) are purely empirical, a theoretical equation for our proposed mass transfer coefficient can be written in terms of fluid-fluid interfacial area, molecular diffusion coefficient, porosity and the thickness of two-film system either side of a fluid-fluid interface (Lewis and Whitman 1924; Seader et al. 2010; Mathias 2024).

While the example utilised in our study focuses on a specific chemical reaction within porous media, it serves as a representative case study to delineate broader challenges and methodologies inherent in modelling reactive transport phenomena. The underlying principles discussed, including the complexities of mixing and dispersion, the challenges in accurately determining reaction rate coefficients and the various modelling approaches employed, are applicable across a wide range of reactive transport scenarios in porous media. By addressing these challenges within the context of a specific case study, we aim to provide valuable insights and solutions that can be extrapolated to other systems and scenarios where mixing, dispersion and reaction play an important role more generally.

2 Mathematical Model

2.1 Conservation of Fluids

Consider one-dimensional flow through a sand column, which is completely saturated with water. The initially residing water (the displaced fluid) is displaced by water injected at an inlet (the displacing fluid). The pore-water velocity in the column is v [LT^{-1}]. Furthermore, due to heterogeneity within the porous structure, the displacing fluid experience dispersion, characterised by a dispersivity, α_L [L]. Let θ_1 [-] and θ_2 [-] be the volume fractions of displaced and displacing fluid, respectively, present within the column; note that $\theta_1 + \theta_2 = 1$. Mass conservation statements for the displaced and displacing fluid take the form

$$\frac{\partial \theta_j}{\partial t} = -\frac{\partial q_j}{\partial x} \quad (1)$$

where t [T] is time, x [L] is distance and

$$q_j = v\theta_j - \alpha_L |v| \frac{\partial \theta_j}{\partial x} \quad (2)$$

Note that $q_1 + q_2 = v$.

2.2 Conservation of Solutes

Suppose there are three solutes in the water. Let C_{ij} [NL^{-3}] be the molar concentration of solute i in phase j . Phase 1 is the displaced fluid and phase 2 is the displacing fluid. A molar conservation statement for solute concentration in this context takes the form

$$\frac{\partial(\theta_j C_{ij})}{\partial t} = -\frac{\partial J_{ij}}{\partial x} - a_{ij} - b_{ij} \quad (3)$$

where

$$J_{ij} = q_j C_{ij} - \alpha_L |q_j| \frac{\partial C_{ij}}{\partial x} \quad (4)$$

and a_{ij} [$\text{NL}^{-3}\text{T}^{-1}$] represents the rate of mass transfer of chemical component, i , from phase j to another phase and b_{ij} [$\text{NL}^{-3}\text{T}^{-1}$] represents the decay of component i in phase j . It follows that

$$\frac{\partial C_{ij}}{\partial t} = \frac{1}{\theta_j} \left[-\frac{\partial J_{ij}}{\partial x} - a_{ij} - b_{ij} - C_{ij} \frac{\partial \theta_j}{\partial t} \right] \quad (5)$$

The total number of moles per unit volume of pore-space of a given component, i , is found from

$$C_i = \theta_1 C_{i1} + \theta_2 C_{i2} \quad (6)$$

2.3 Initial and Boundary Conditions

Gramling's experiment is represented by applying the following initial and boundary conditions:

$$\left\{ \begin{array}{ll} \theta_1 = 1, & 0 \leq x \leq L, t = 0 \\ \theta_2 = 0, & 0 \leq x \leq L, t = 0 \\ C_{11} = C_0, & 0 \leq x \leq L, t = 0 \\ C_{21} = C_{31} = C_{12} = C_{22} = C_{32} = 0, & 0 \leq x \leq L, t = 0 \\ q_1 = 0, & x = 0, t > 0 \\ q_2 = v, & x = 0, t > 0 \\ J_{11} = J_{21} = J_{31} = J_{12} = J_{32} = 0, & x = 0, t > 0 \\ J_{22} = vC_0, & x = 0, t > 0 \\ \frac{\partial \theta_1}{\partial x} = \frac{\partial \theta_2}{\partial x} = 0, & x = L, t > 0 \\ \frac{\partial C_{11}}{\partial x} = \frac{\partial C_{21}}{\partial x} = \frac{\partial C_{31}}{\partial x} = \frac{\partial C_{12}}{\partial x} = \frac{\partial C_{22}}{\partial x} = \frac{\partial C_{32}}{\partial x} = 0, & x = L, t > 0 \end{array} \right. \quad (7)$$

where C_0 [NL^{-3}] is the initial molarity of both reactants associated with Gramling's experiment, and L [L] is the length of the sand column.

2.4 Bimolecular Equilibrium Reaction

Gramling's bimolecular reactive transport experiment involved the following reaction process (Gramling et al. 2002)



Letting components 1, 2 and 3 be $\text{Na}_2\text{EDTA}^{2-}$, $\text{CuSO}_4(\text{aq})$ and CuEDTA^{2-} , respectively, the bimolecular reaction described in Eq. (8) can be represented using the following decay rate expressions

$$b_{1j} = b_{2j} = -b_{3j} = B_{1j}H(C_{2j} - C_{1j}) + B_{2j}H(C_{1j} - C_{2j}) \quad (9)$$

where

$$B_{ij} = -\frac{\partial J_{ij}}{\partial x} - a_{ij} \quad (10)$$

and $H(x)$ denotes the Heaviside step function.

The mass of CuEDTA^{2-} produced, m_3 [M], is found from

$$m_3 = A\phi M_3 \left\{ \int_0^L [\theta_1 C_{31} + \theta_2 C_{32}] dx + \int_0^t [J_{31}(x=L, t) + J_{32}(x=L, t)] dt \right\} \quad (11)$$

where A [L^2] is the cross-sectional area of the sand column, ϕ [-] is the effective porosity and M_3 [MN^{-1}] is the molecular weight of CuEDTA^{2-} (according to Alhashmi et al. (2015), this is $351.75 \text{ g mol}^{-1}$).

2.5 Two-Film Mass Transfer Model

The mass transfer terms are found from

$$a_{i1} = -a_{i2} = k(C_{i1} - C_{i2}) \quad (12)$$

where k [T^{-1}] is the apparent mass transfer coefficient defined by (consider Seader et al. (2010, p. 124) or Mathias (2023, p. 600))

$$k = \frac{\beta D_0}{2\phi b} \quad (13)$$

where β [L^{-1}] is the fluid-fluid interfacial area per unit volume of porous media, D_0 [L^2T^{-1}] is the molecular diffusion coefficient and b [L] is the thickness of a two-film system either side of the displaced and displacing fluid interface.

In practice, k can be treated as an empirical parameter. The presence of multiple mass transfer timescales, often present in natural porous media, tends to lead to a strong correlation between overall mass transfer rate with observation duration (Haggerty et al. 2004). Following the suggestions of Sanchez-Vila et al. (2010), Zhang et al. (2013) and Ginn (2018), we will take k to be a declining function with time of the form

$$k = k_0 t^{-\eta} \quad (14)$$

where k_0 [$\text{T}^{\eta-1}$] and η [-] are empirical parameters to be found by calibration. Note that k_0 and η are the only additional parameters required, on top of those already needed to use Gramling's original ADE model.

2.6 Numerical Solution

Noting again that $\theta_1 = 1 - \theta_2$, it can be understood that the above set of equations requires the solution of seven coupled partial differential equations (PDE). The primary dependant variables include θ_2 , C_{11} , C_{21} , C_{12} , C_{22} , C_{31} and C_{32} . Accurate numerical solutions can be obtained by the method of lines. Here we will discretise in space using finite differences

and, following Goudarzi et al. (2016), solve the resulting set of coupled ordinary differential equations (ODE) with respect to time using MATLAB's stiff ODE solver, ODE15s (Shampine and Reichelt 1997; Shampine and Thompson 2001). Spatial discretisation is achieved using a uniform space-step of 1 mm. Numerical diffusion is avoided by using central differencing for first-order derivatives. The global mass balance for the three components is verified (and has been confirmed) using the solver flux output method described by Ireson et al. (2023).

A grid convergence study was performed for the simulation presented in Fig. 6c. It was found that our numerical solution produced close to indistinguishable results when space-steps of 2 mm, 1 mm and 0.5 mm were used. Therefore it was concluded that a space-step of 1 mm should be sufficiently small for all the other simulations performed.

2.7 Analytical Solutions for Equilibrium Mass Transfer

For the special case when the mass transfer process between the displaced and displacing fluids can be treated as an equilibrium process (i.e., when $k_0 \rightarrow \infty$), the following analytical solutions apply (Gramling et al. 2002):

$$C_1 \equiv \theta_1 C_{11} + \theta_2 C_{12} = C_0 \left[1 - \frac{1}{2} \operatorname{erfc} \left(\frac{x - vt}{2\sqrt{\alpha_L vt}} \right) \right] \quad (15)$$

$$C_2 \equiv \theta_1 C_{21} + \theta_2 C_{22} = \frac{C_0}{2} \operatorname{erfc} \left(\frac{x - vt}{2\sqrt{\alpha_L vt}} \right) \quad (16)$$

$$C_3 \equiv \theta_1 C_{31} + \theta_2 C_{32} = C_1 H(C_2 - C_1) + C_2 H(C_1 - C_2) \quad (17)$$

$$m_3 = 2A\phi C_0 M_3 \sqrt{\frac{\alpha_L vt}{\pi}} \quad (18)$$

3 Experimental Data

We will use experimental data from Gramling et al. (2002) to verify our proposed modeling approach. Gramling et al. (2002) performed six tracer tests on a 36 cm long sand column. Three non-reactive tracer tests were performed by displacing a 0.02 M $\text{Na}_2\text{EDTA}^{2-}$ solution with a 0.01 M CuEDTA^{2-} solution at flow rates, Q [L^3T^{-1}], of 2.67, 16 and 150 ml min^{-1} . Three reactive tracer tests were performed by displacing a 0.02 M $\text{Na}_2\text{EDTA}^{2-}$ with a 0.01 M $\text{CuSO}_4(\text{aq})$ solution at flow rates of 2.67, 16 and 150 ml min^{-1} .

For the reactive tracer tests, contact of the displacing fluid with the displaced fluid leads to the reaction described in Eq. (8). The physical colour of $\text{CuSO}_4(\text{aq})$ and CuEDTA^{2-} are light blue and dark blue, respectively. The spatial distribution of solute concentration for these two components was measured using a transmitted light imaging technique. Gramling et al. (2002) calibrated the analytical solution for C_1 , given by Eq. (15), to CuEDTA^{2-} concentration profiles from the non-reactive transport experiments to obtain estimates of

Table 1 Relevant parameter values describing the three reactive transport experiments of Gramling et al. (2002)

Flow rate, Q (ml min ⁻¹)	2.67	16	150
Column length, L (cm)	36	36	36
Cross-sectional area, A (cm ²)	5.5×1.8	5.5×1.8	5.5×1.8
Effective porosity, ϕ (-)	0.36	0.36	0.36
Boundary molarity of reactant, C_0 (mol m ⁻³)	0.02	0.02	0.02
Pore-water velocity, v (cm s ⁻¹)	1.21×10^{-2}	8.32×10^{-2}	6.7×10^{-1}
Dispersion coefficient, D_L (cm ² s ⁻¹)	1.75×10^{-3}	1.45×10^{-2}	1.75×10^{-1}
Dispersivity, α_L (cm)	0.145	0.174	0.261
Kinematic porosity, ϕ_k (-)	0.371	0.324	0.377

pore-water velocity, v [LT⁻¹], and longitudinal dispersion coefficient, $D_L = \alpha_L |v|$ [L], for use in analysing the three corresponding reactive transport experiments. Relevant parameter values describing the three reactive transport experiments are listed in Table 1. Note that the kinematic porosity, $\phi_k = \frac{Q}{Av}$, comes out larger than the effective porosity for both the 2.67 ml min⁻¹ and 150 ml min⁻¹ scenarios.

Gramling et al. (2002) report spatial CuEDTA²⁻ concentration profiles within the sand column after 619, 916, 1114 and 1510 s for the 2.67 ml min⁻¹ experiment, after 157 s for the 16 ml min⁻¹ experiment and after 20.23 s for the 150 ml min⁻¹ experiment. Additionally, Gramling et al. (2002) report time-series data for CuEDTA²⁻ production for each of the three experiments in their Fig. 6. We will use all of this data to evaluate the performance of our proposed model.

3.1 Re-scaling Gramling's CuEDTA²⁻ Production Data

While Edery et al. (2010), Sanchez-Vila et al. (2010) and Zhang et al. (2013) present convincing correspondence between their models and Gramling's CuEDTA²⁻ production data, Alhashmi et al. (2015) dismiss this data due to a significant mass balance discrepancy. It is unfortunate not to use this data because it provides important information about the early-time response of the experiments, not captured by the spatial concentration distribution data.

Gramling et al. (2002) plotted results from their analytical solution (Eq. 18) alongside the observed CuEDTA²⁻ production data, which display a similar inconsistency. It is therefore possible to determine an appropriate scaling factor to correct the CuEDTA²⁻ production data by comparing results from Eq. (18) with the corresponding results plotted by Gramling et al. (2002). Figure 1 shows plots of uncorrected and corrected observed CuEDTA²⁻ production data against number of pore volumes injected for the three flow rates studied by Gramling et al. (2002), based on such a comparison. The number of pore volumes injected is hereafter referred to as "pore volume" or PV. Note that

$$PV = \frac{Qt}{AL\phi} \quad (19)$$

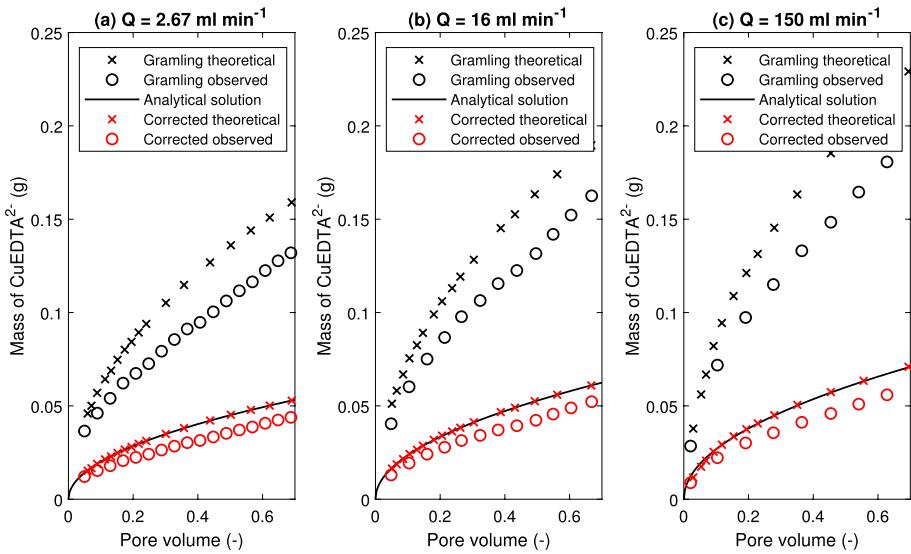


Fig. 1 Plots of theoretical and observed produced mass of CuEDTA^{2-} against pore volume for the three flow rates studied by Gramling et al. (2002): **a** 2.67 ml min^{-1} , **b** 16 ml min^{-1} , **c** 150 ml min^{-1} . The data identified, in the legend, with Gramling was obtained directly from Figure 6 of Gramling et al. (2002). The solid black lines were determined from Eq. (18). The data identified, in the legend, as “corrected” was obtained by scaling Gramling’s data such that their theoretical results have the same mean as that of the analytical solution (black solid line)

4 Results

4.1 Non-reactive Transport Examples

Figure 2 shows results from the numerical solution described in Sect. 2.6 but for a non-reactive substance. The reaction in our model is easily switched off by setting the b_{ij} terms to zero. The scenario shown in Fig. 2 was obtained using parameter values from Table 1 for the 2.67 ml min^{-1} scenario. The η parameter in Eq. (14) was set to zero with model sensitivity explored by varying the k_0 parameter.

The first thing to notice is that the θ_2 values from the numerical solution (the solid lines) correspond exactly with the C_2/C_0 values from the analytical solution given by Eq. (16) (the circular markers). This is because the mass transfer terms, a_{ij} , only feature in the transport equations for C_{ij} and do not feature in the mass conservation statements for the fluids (recall Eq. 1).

The second thing to notice is that the C_2/C_0 values from the numerical solution (the small circular dots) also correspond exactly with the C_2/C_0 values from the analytical solution given by Eq. (16) (the circular markers). This is because there is no reaction and so when you add together the two phase components (recall $C_2 = \theta_1 C_{21} + \theta_2 C_{22}$), the effect of the mass transfer process between the two fluid phases becomes irrelevant.

Nevertheless, the concentrations of component 2 are greater in the displacing fluid (the C_{22} values shown as dash-dot lines) than they are in the displaced fluid (the C_{21}

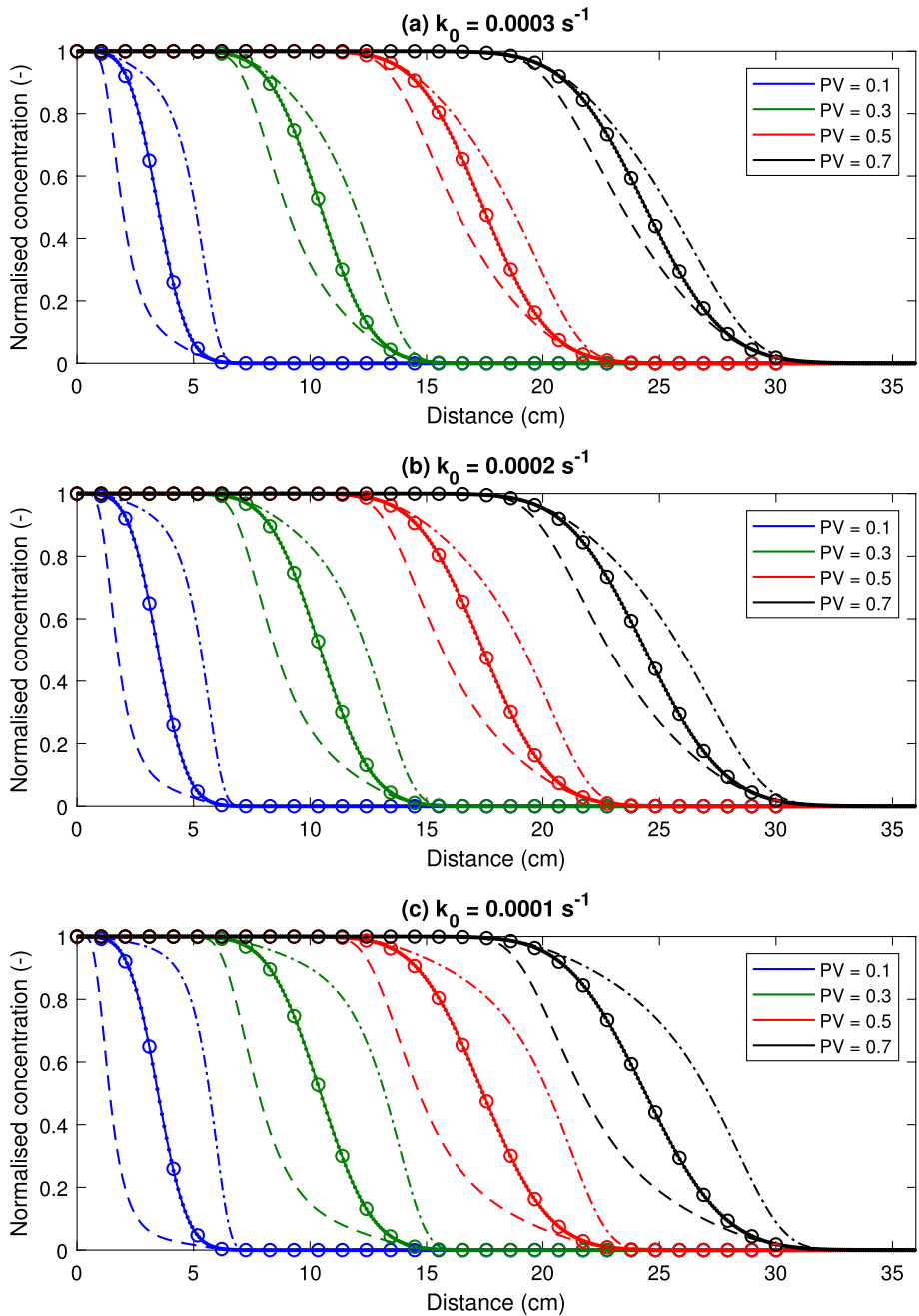


Fig. 2 Plots of normalised concentration, for a non-reactive substance, against distance for various pore volume (PV) with $Q = 2.67 \text{ ml min}^{-1}$. **a–c** show results for when $k_0 = 0.0003 \text{ s}^{-1}$, 0.0002 s^{-1} and 0.0001 s^{-1} , respectively, with $\eta = 0$. The dashed, solid and dash-dot lines are results for $C_{21}/C_0, \theta_2$ and C_{22}/C_0 , respectively. The small circular dots are results for C_2/C_0 . The circular open markers are results from the analytical solution, Eq. (16)

values shown as dashed lines). The space between the dashed and dash-dot lines represent an incompletely mixed zone (IMZ) that exists around the displaced and displacing fluid interface (indicated by the solid lines). The IMZ decreases in size with increasing k_0 because the k_0 value controls the rate at which the displacing and displaced fluids are mixed together. The IMZ decreases in size with increasing time (or pore volume) because the more time that has passed, the greater the extent of mixing that has taken place.

4.2 Reactive Transport Examples

Figures 3 and 4 compare results from the numerical solution (as described in Sect. 2.6) with the analytical solutions, Eqs. (17) and (18) (which represent the limiting case when $k_0 \rightarrow \infty$), and observed data from Gramling's experiments for each of the three flow rates studied. Figure 3 shows the sensitivity of the model to k_0 with $\eta = 0$. Figure 4 shows the sensitivity of the model to k_0 with $\eta = 1$. All other parameters were as specified in Table 1.

For a given pore volume (or time), the total number of moles of CuEDTA^{2-} per unit volume of pore-space, C_3 , presents as a bell-shaped distribution with distance from the inlet (see Figs. 3a, c and e or 4a, c and e). In contrast, the analytical solution (Eq. 17) presents with a spiked central peak. Results from the numerical solution are found to asymptotically approach the results from the analytical solution either side of this central peak. However, the effect of decreasing the k_0 value leads to a smoothing out of this central peak. A reduction in the central peak value implies a reduction in the production of CuEDTA^{2-} , which comes about due to an increase in the size of the IMZ (consider again Fig. 2).

When $\eta = 0$ it is found that the value of k_0 required, to sufficiently suppress the central spike such that the model results better correspond with Gramling's experimental observations, varies by orders of magnitude for each of the flow rates studied. When $Q = 2.67 \text{ ml min}^{-1}$, k_0 needs to be around 0.0002 s^{-1} . When $Q = 16 \text{ ml min}^{-1}$, k_0 needs to be around 0.002 s^{-1} . When $Q = 150 \text{ ml min}^{-1}$, k_0 needs to be around 0.02 s^{-1} .

As mentioned in Sect. 1, Sanchez-Vila et al. (2010) employed a reaction rate coefficient that declined as a power law with time. Through seeking to match their model with Gramling's data, they found an exponent (analogous to our η parameter) of 0.93 was required. We set $\eta = 1$ to obtain Fig. 4 with this in mind. Setting $\eta = 1$ leads to a more uniform k_0 requirement for the different flow rates studied, with optimal results (to one significant figure) achieved with $k_0 = 0.2 \text{ s}^0$ (recall that the dimensions of k_0 are dictated by the value of η adopted).

Figure 3b, d and f show plots of produced mass of CuEDTA^{2-} against pore volume for each of the flow rates studied with $\eta = 0$. It can be seen that none of the model results correspond well with the observed data from Gramling et al. (2002). The analytical solution overestimates the mass of CuEDTA^{2-} produced. In contrast, the numerical solutions start off by significantly underestimating the rate of CuEDTA^{2-} production and then appear to asymptotically converge with the analytical solution for later times (larger pore volume). Recall that the size of the IMZ reduces with time (consider again Fig. 2a). During early times, the IMZ suppresses CuEDTA^{2-} production. During later times, the IMZ becomes sufficiently small such that the numerical solution converges on to the results for the analytical solution.

Figure 4a, c and e show plots of produced mass of CuEDTA^{2-} against pore volume for each of the flow rates studied with $\eta = 1$. All of the numerical solutions start off with similar behaviour to the analytical solution. This is because the apparent mass transfer rate,

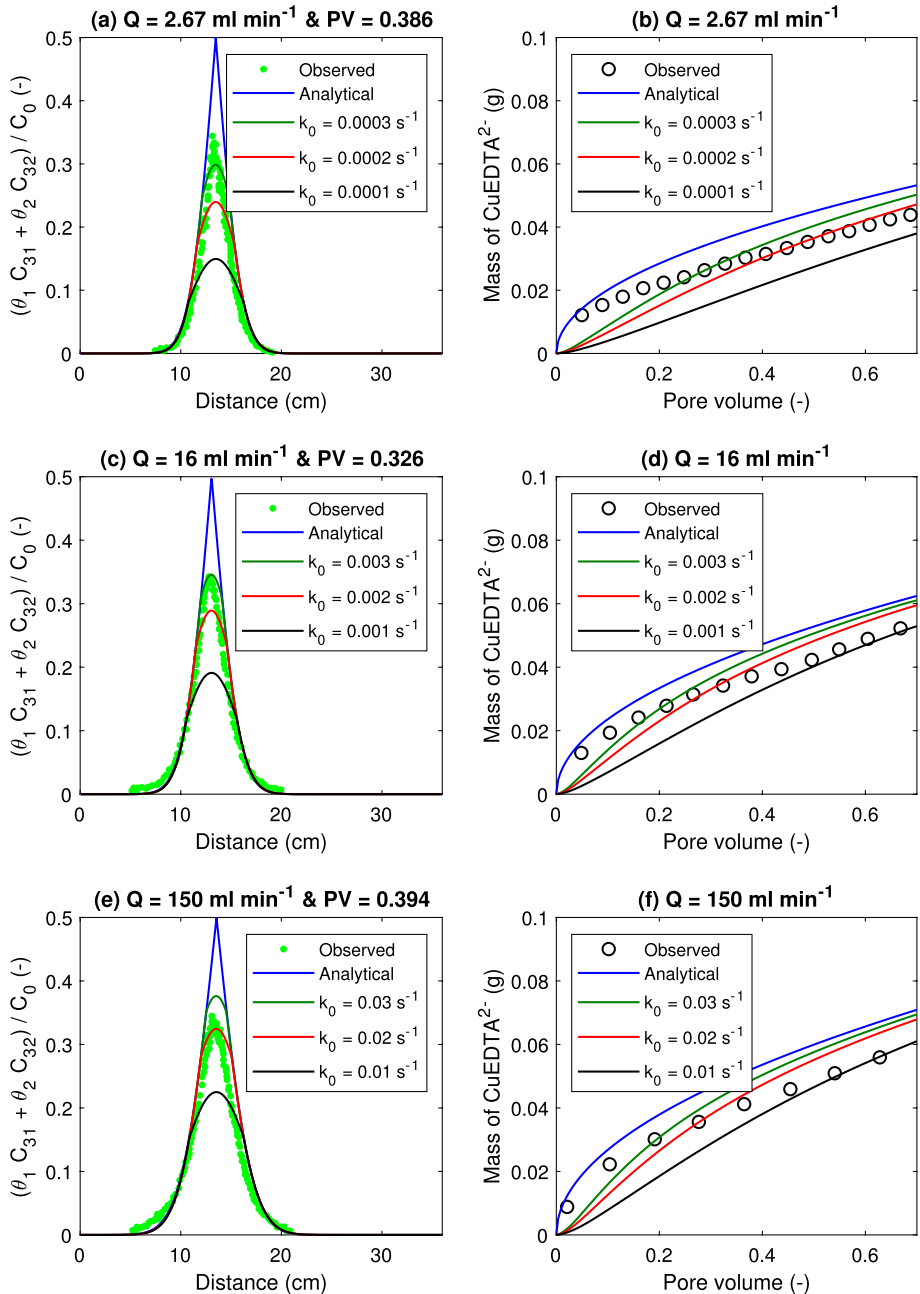


Fig. 3 Sensitivity analysis with $\eta = 0$. **a**, **c** and **e** show plots of normalised CuEDTA²⁻ concentration against distance for a specified pore volume (PV) with $Q = 2.67 \text{ ml min}^{-1}$, 16 ml min^{-1} and 150 ml min^{-1} , respectively. **b**, **d** and **f** show plots of produced mass of CuEDTA²⁻ against pore volume for $Q = 2.67 \text{ ml min}^{-1}$, 16 ml min^{-1} and 150 ml min^{-1} , respectively. The circular markers are the observed data from Gramling et al. (2002), the blue lines are from the analytical solution (Eqs. 17 and 18), the other lines are from the numerical solution (Sect. 2.6) with varying k_0 value as indicated in the legends

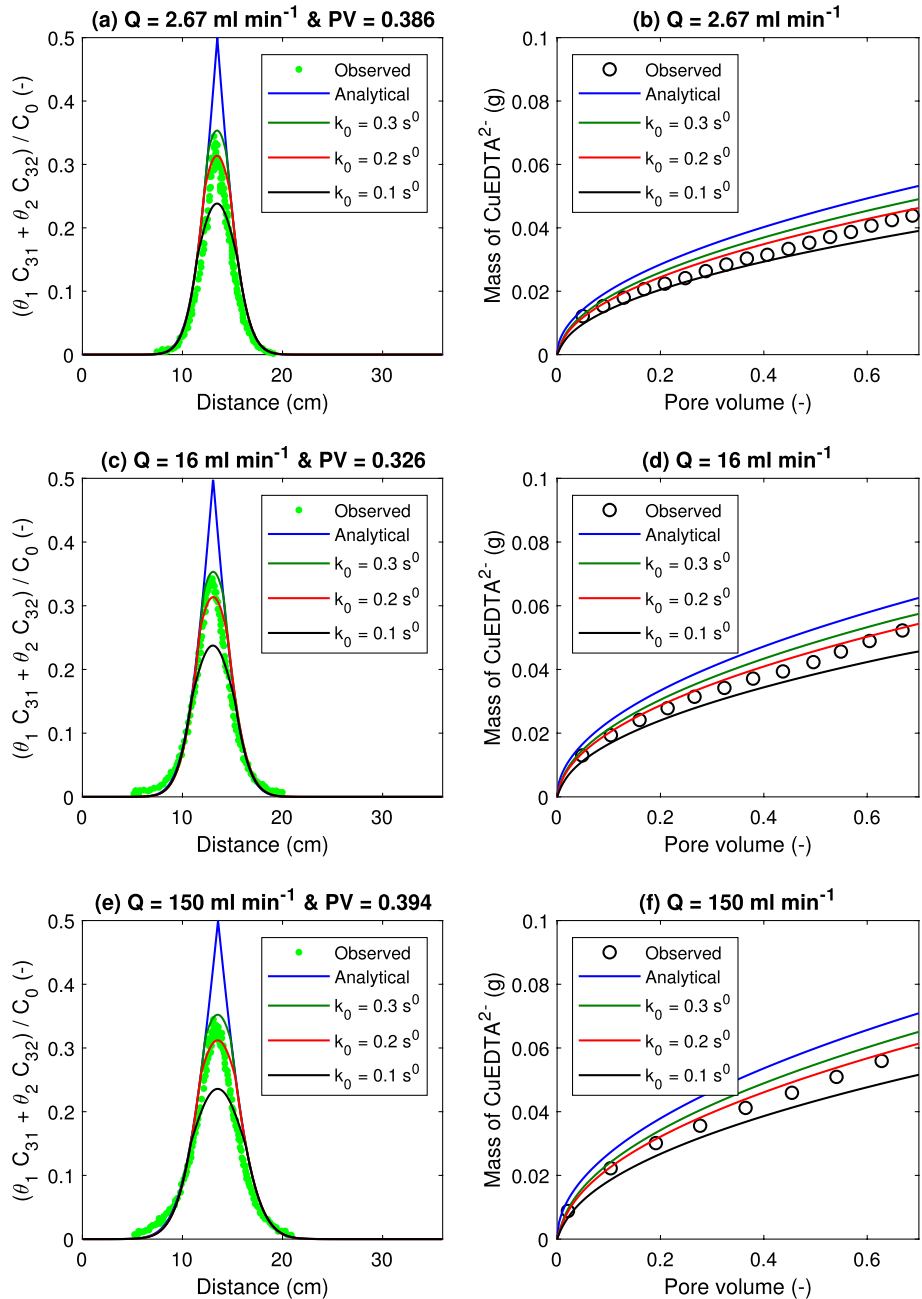


Fig. 4 Sensitivity analysis with $\eta = 1$. **a**, **c** and **d** show plots of normalised CuEDTA²⁻ concentration against distance for a specified pore volume with $Q = 2.67 \text{ ml min}^{-1}$, 16 ml min^{-1} and 150 ml min^{-1} , respectively. **b**, **d** and **f** show plots of produced mass of CuEDTA²⁻ against pore volume for $Q = 2.67 \text{ ml min}^{-1}$, 16 ml min^{-1} and 150 ml min^{-1} , respectively. The circular markers are the observed data from Gramling et al. (2002), the blue lines are from the analytical solution (Eqs. 17 and 18), the other lines are from the numerical solution (Sect. 2.6) with varying k_0 value as indicated in the legends

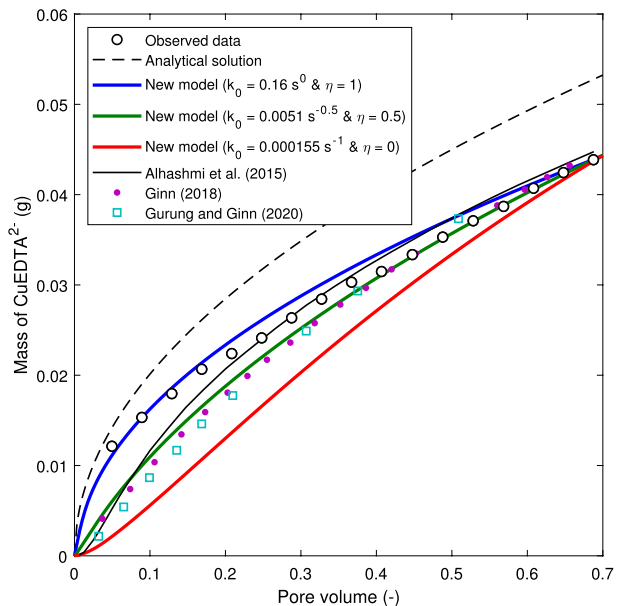
k , is close to infinity during early times by virtue of its relationship with time (through the selection of a non-zero value of η). The numerical solutions provide progressively less CuEDTA^{2-} with time as compared to the analytical solution. This is because the k value progressively reduces, which lead to a progressively larger IMZ. In this context, it is found that a value of $k_0 = 0.2 \text{ s}^0$ also provides a reasonable correspondence between the numerical solution and Gramling's CuEDTA^{2-} production data for all three flow rates studied.

As mentioned earlier, Sanchez-Vila et al. (2010) adopted a rate coefficient that declined as a power law of time with an exponent (analogous to η) of 0.93. In contrast, Zhang et al. (2013), Ginn (2018) and Gurung and Ginn (2020) adopted an analogous exponent of 0.5. Comparing the results shown in Figs. 3 and 4 it can be understood that the impact of a specific k_0 value on concentration profiles is strongly dependent on the specified value of η . To explore the impact of η further, we searched for values of k_0 , for when $\eta = 1$, $\eta = 0.5$ and $\eta = 0$, such that our numerical solution produces the same mass of CuEDTA^{2-} , observed by Gramling et al. (2002), after 0.7 pore volume when $Q = 2.67 \text{ ml min}^{-1}$. A comparison of simulated and observed CuEDTA^{2-} production values is presented in Fig. 5, with the calibrated k_0 values reported in the legend.

When $\eta = 0$, the numerical solution underestimates the CuEDTA^{2-} mass production for all times less than 0.7 pore volume. When $\eta = 0.5$, the numerical solution underestimates the CuEDTA^{2-} mass production for all times less than 0.4 pore volume but more closely matches the observed data thereafter. When $\eta = 1$, the numerical solution is able to much more closely follow the observed production data during early times (i.e., less than 0.2 pore volume) as compared to when $\eta = 0.5$ or $\eta = 0$.

Figure 5 also shows the simulated CuEDTA^{2-} mass production data from Alhashmi et al. (2015), Ginn (2018) and Gurung and Ginn (2020) for comparison purposes. The simulated data from our model with $\eta = 0.5$ closely follows that of Ginn (2018) and Gurung and Ginn (2020), which is not surprising because their models assumed their rate coefficients declined with a square root of time. The advantage of our model over that of Ginn

Fig. 5 Plots of produced mass of CuEDTA^{2-} against pore volume for the 2.67 ml min^{-1} scenario. The black circular markers are the observed data from Gramling et al. (2002), the black dashed line is from the analytical solution, Eq. (18), the blue, green and red solid lines are from our numerical solution with k_0 and η values as shown in the legend, the black solid line, magenta circular markers and turquoise square markers are from the models of Alhashmi et al. (2015), Ginn (2018) and Gurung and Ginn (2020), respectively



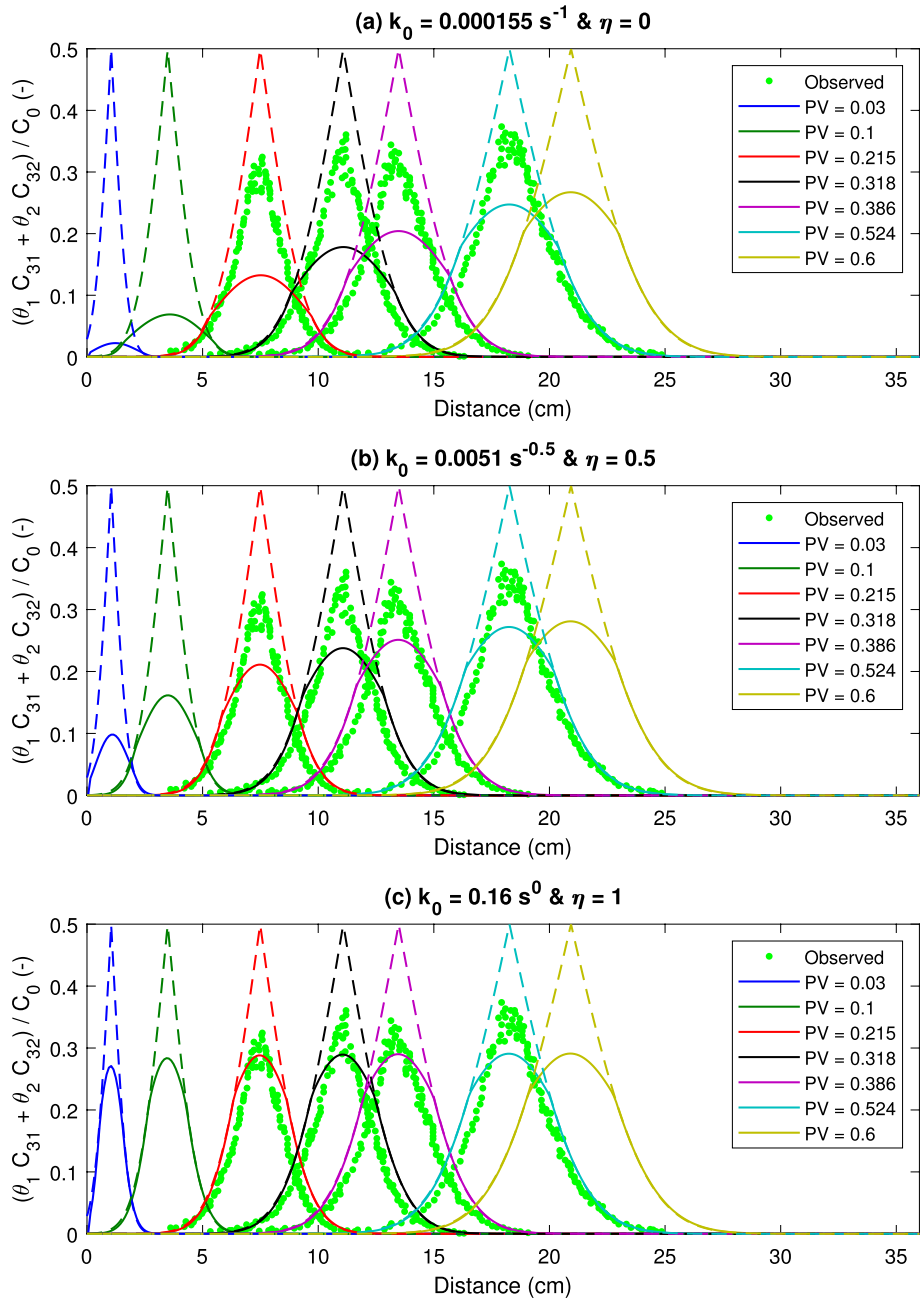


Fig. 6 Plots of normalised CuEDTA^{2-} concentration against distance with $Q = 2.67 \text{ ml min}^{-1}$ for various pore volume (PV). The green markers are the observed data from Gramling et al. (2002), the solid lines are from the numerical solution (Sect. 2.6) and the dashed lines are from the analytical solution (Eq. 17). **a–c** show results from the numerical solution with different k_0 and η values as indicated in the subtitles

(2018) and Gurung and Ginn (2020) is that it avoids the need to treat the mixing process as a kinetic reaction process and instead invokes Whitman's classical two-film mass transfer model.

Figure 6 shows plots of normalised CuEDTA^{2-} concentration against distance for different pore volume with $\eta = 0$, $\eta = 0.5$ and $\eta = 1$ along with the associated k_0 values used to obtain Fig. 5. When $\eta = 0$, the simulated peak CuEDTA^{2-} concentration increases with increasing PV but is always much less than that observed by Gramling et al. (2002). The reason the peak concentration increases with increasing PV is due to the size of the IMZ decreasing with time. The reason the simulated peak concentrations are much lower than those observed by Gramling et al. (2002) is that the k_0 value needs to be very high to ensure the total mass of CuEDTA^{2-} produced is matched to the observed production data after 0.7 PV. When $\eta = 1$, the simulated peak CuEDTA^{2-} concentration remains the same with increasing PV and is always much closer to that observed by Gramling et al. (2002), as compared to the $\eta = 0$ simulation. The reason the peak concentrations remain more steady is that the k_0 value progressively increases giving rise to a much more slowly declining size of the IMZ (as compared to the $\eta = 0$ simulation). When $\eta = 0.5$, the simulated CuEDTA^{2-} concentrations exhibit an intermediate response between those observed from the $\eta = 1$ and $\eta = 0$ models.

Regardless of the choice of η value, it is found that the simulated peak CuEDTA^{2-} concentrations are always lower than those observed by Gramling et al. (2002). This is because our spatial concentration profiles are over-dispersed and so the peak values must be underestimated to match the total mass of CuEDTA^{2-} produced, as in Fig. 5. The dispersion of the profiles is controlled by the dispersion coefficient and we have used the value reported in Table 1. Gramling et al. (2002) obtained this value by calibrating the analytical solution, Eq. (16), to a set of corresponding non-reactive experimental data.

Both Sanchez-Vila et al. (2010) and Zhang et al. (2013) chose to reduce Gramling's dispersion coefficient from $1.75 \times 10^{-3} \text{ cm}^2 \text{ s}^{-1}$ to $1.3 \times 10^{-3} \text{ cm}^2 \text{ s}^{-1}$. Whilst this tightens their model around peak concentrations it leads to overestimates of CuEDTA^{2-} concentration in the upstream and downstream tails (see Figure 1 of Sanchez-Vila et al. 2010 and Figure 11 of Zhang et al. 2013), which is a problem, because this region is far away from the IMZ and should be where our models collectively work the best. Instead, we prefer to accept that: (1) whilst our new two-film model significantly improves the physical representation of IMZs within classical continuum scale models, the possibility of improvement remains; and/or (2) there may be significant and unaccounted measurement uncertainty associated with the observed data we are comparing to.

5 Summary and Conclusions

Reliable reactive transport models require careful separation of mixing and dispersion processes. Previous studies have focused on the use of kinetic reaction models to account for incomplete mixing. The objective of our study was to treat the displacing and displaced fluids as two separate fluid phases and to then invoke Whitman's classical two-film theory, to model mass transfer between the two phases. We used experimental data from Gramling's bimolecular reaction experiment (Gramling et al. 2002) to assess model performance. Gramling's original model involved just three coupled PDEs. In this context, our new formulation leads to a set of seven coupled PDEs but only requires the specification of two

extra parameters, associated with the mass transfer coefficient and its dependence on time (i.e., k_0 and η).

Our first set of simulations focused on how the two-film theory affects non-reactive transport. For simplicity we set $\eta = 0$ (which implies that the mass transfer coefficient is constant with time) and varied k_0 . It was found that the concentration of a tracer in the displacing fluid was always higher in the displacing fluid as compared to the displaced fluid. When plotting these two concentrations against distance they form an envelope around a plot of the volume fraction of displacing fluid. This envelope can be thought of as an incompletely mixed zone (IMZ). The size of this IMZ was found to decrease with increasing k_0 value and increasing time.

Our second set of simulations focused on how the two film theory affects transport in the presence of Gramling's bimolecular reaction. The reaction process leads to the production of CuEDTA^{2-} , which presents as a bell-shaped concentration distribution with distance from the displacing fluid inlet. Gramling's original analytical solution gives rise to a spiked central peak in CuEDTA^{2-} concentration. Increasing k_0 value in our new model leads to an increasing sized IMZ. This in turn, suppresses the production of CuEDTA^{2-} and hence also the magnitude of the central peak concentration, such that our model corresponds much better with Gramling's experimental observations.

It was found that assuming a constant mass transfer coefficient (i.e., assuming $\eta = 0$) led to an underestimate in CuEDTA^{2-} production during early times and an overestimate during later times. By setting $\eta = 0.5$, the mass transfer coefficient declined with time, leading to results that were close to identical to those previously presented by Ginn (2018) and Gurung and Ginn (2020). Improved conformance with Gramling's experimental data was further achieved by setting $\eta = 1$.

The use of a time-dependent reaction rate coefficient (Sanchez-Vila et al. 2010; Zhang et al. 2013; Ginn 2018; Gurung and Ginn 2020) has previously been justified by the experimental finding of Haggerty et al. (2004), that heterogeneity in mass transfer coefficients often manifests as a time-varying mass transfer coefficient at larger spatial scales. However, mass transfer and reaction kinetics are clearly very different processes. In contrast, our time-varying two-film mass transfer coefficient is very much in the spirit of the ideas and processes discussed by Haggerty et al. (2004).

The two film mass transfer model provides a simple and theoretically based method for separating mixing from dispersion in Eulerian continuum-scale methods. The advantage of this approach over existing methods is that it enables the simulation of equilibrium chemical reactions without having to invoke unrealistically small reaction rate coefficients. The comparison with Gramling's experimental data confirms that our proposed method is suitable for simulating realistic and complicated bimolecular reaction behaviour. However, further work is needed to explore alternative methods for avoiding the need of a time-dependent mass transfer rate coefficient, possibly involving the development of a multi-rate extension (consider, for example, the work of Mathias et al. (2020)).

Author Contributions All authors contributed to the study conception and design. Material preparation, data collection and analysis were performed by Simon Mathias. The first draft of the manuscript was written by Simon Mathias and all authors commented on previous versions of the manuscript. All authors read and approved the final manuscript.

Funding The authors declare that no funds, grants, or other support were received during the preparation of this manuscript.

Data Availability Statement The datasets generated during and/or analysed during the current study are available from the corresponding author on reasonable request.

Declarations

Conflict of interest The authors have no relevant financial or non-financial interests to disclose.

Open Access This article is licensed under a Creative Commons Attribution 4.0 International License, which permits use, sharing, adaptation, distribution and reproduction in any medium or format, as long as you give appropriate credit to the original author(s) and the source, provide a link to the Creative Commons licence, and indicate if changes were made. The images or other third party material in this article are included in the article's Creative Commons licence, unless indicated otherwise in a credit line to the material. If material is not included in the article's Creative Commons licence and your intended use is not permitted by statutory regulation or exceeds the permitted use, you will need to obtain permission directly from the copyright holder. To view a copy of this licence, visit <http://creativecommons.org/licenses/by/4.0/>.

References

- Alhashmi, Z., Blunt, M.J., Bijeljic, B.: Predictions of dynamic changes in reaction rates as a consequence of incomplete mixing using pore scale reactive transport modeling on images of porous media. *J. Contam. Hydrol.* **179**, 171–181 (2015)
- Barnard, J.M.: Simulation of mixing-limited reactions using a continuum approach. *Adv. Water Resour.* **104**, 15–22 (2017)
- Diersch, H.J.G.: *FEFLOW: finite element modeling of flow, mass and heat transport in porous and fractured media*. Springer, Berlin (2013)
- Ding, D., Benson, D.A., Paster, A., Bolster, D.: Modeling bimolecular reactions and transport in porous media via particle tracking. *Adv. Water Resour.* **53**, 56–65 (2013)
- Edey, Y., Scher, H., Berkowitz, B.: Modeling bimolecular reactions and transport in porous media. *Geophys. Res. Lett.* **36**(2) (2009)
- Edey, Y., Scher, H., Berkowitz, B.: Particle tracking model of bimolecular reactive transport in porous media. *Water Resour. Res.* **46**(7) (2010)
- Ginn, T.R.: Modeling bimolecular reactive transport with mixing-limitation: theory and application to column experiments. *Water Resour. Res.* **54**(1), 256–270 (2018)
- Goudarzi, S., Mathias, S.A., Gluyas, J.G.: Simulation of three-component two-phase flow in porous media using method of lines. *Transp. Porous Media* **112**(1), 1–19 (2016)
- Gramling, C.M., Harvey, C.F., Meigs, L.C.: Reactive transport in porous media: a comparison of model prediction with laboratory visualization. *Environ. Sci. Technol.* **36**(11), 2508–2514 (2002)
- Gurung, D., Ginn, T.R.: Mixing ratios with age: application to preasymptotic one-dimensional equilibrium bimolecular reactive transport in porous media. *Water Resour. Res.* **56**(7), e2020WR027629 (2020)
- Haggerty, R., Harvey, C. F., Freiherr von Schwerin, C., Meigs, L.C.: What controls the apparent timescale of solute mass transfer in aquifers and soils? A comparison of experimental results. *Water Resour. Res.* **40**(1) (2004)
- Ireson, A.M., Spiteri, R.J., Clark, M.P., Mathias, S.A.: A simple, efficient, mass-conservative approach to solving Richards' equation (openRE, v1. 0). *Geosci. Model Dev.* **16**(2), 659–677 (2023)
- Jung, Y., Pau, G.S.H., Finsterle, S., Pollyea, R.M.: TOUGH3: a new efficient version of the TOUGH suite of multiphase flow and transport simulators. *Comput. Geosci.* **108**, 2–7 (2017)
- Lewis, W.K., Whitman, W.G.: Principles of gas absorption. *Ind. Eng. Chem.* **16**(12), 1215–1220 (1924)
- Mathias, S.A.: *Hydraulics. Hydrology and Environmental Engineering*, Springer, Berlin (2023). <https://doi.org/10.1007/978-3-031-41973-7>
- Mathias, S.A., Dentz, M., Liu, Q.: Gas diffusion in coal powders is a multi-rate process. *Transp. Porous Media* **131**, 1037–1051 (2020)
- Sanchez-Vila, X., Fernández-García, D., Guadagnini, A.: Interpretation of column experiments of transport of solutes undergoing an irreversible bimolecular reaction using a continuum approximation. *Water Resour. Res.* **46**(12) (2010)
- Seader, J.D., Henley, E.J., Roper, D.K.: *Separation Process Principles*, 3rd edn. Wiley, New York (2010)
- Shampine, L.F., Reichelt, M.W.: The MATLAB ODE suite. *SIAM J. Sci. Comput.* **18**(1), 1–22 (1997)
- Shampine, L.F., Thompson, S.: Solving DDEs in MATLAB. *Appl. Numer. Math.* **37**(4), 441–458 (2001)
- Simunek, J., Van Genuchten, M.T., & Sejna, M. (2016). Recent developments and applications of the HYDRUS computer software packages. *Vadose Zone J.* **15**(7)

- Sole-Mari, G., Fernández-García, D., Sanchez-Vila, X., Bolster, D.: Lagrangian modeling of mixing-limited reactive transport in porous media: multirate interaction by exchange with the mean. *Water Resour. Res.* **56**(8), e2019WR026993 (2020)
- Sole-Mari, G., Bolster, D., Fernandez-Garcia, D.: A closer look: High-resolution pore-scale simulations of solute transport and mixing through porous media columns. *Transp. Porous Media* 1–27 (2022)
- Voss, C.I., Provost, A.M.: SUTRA A model for saturated-unsaturated, variable-density ground-water flow with solute or energy transport. Water-Resources Investigations Report 02-4231. U. S. Geological Survey (2010). <https://www.usgs.gov/software/sutra-a-model-2d-or-3d-saturated-unsaturated-variable-density-ground-water-flow-solute-or>. Accessed 31, 08 2023
- Zhang, Y., Papelis, C., Sun, P., Yu, Z.: Evaluation and linking of effective parameters in particle-based models and continuum models for mixing-limited bimolecular reactions. *Water Resour. Res.* **49**(8), 4845–4865 (2013)

Publisher's Note Springer Nature remains neutral with regard to jurisdictional claims in published maps and institutional affiliations.